Upwind Formulations for the Euler Equations in Steady Supersonic Flows

Nicola Botta* and Maurizio Pandolfi†
Politecnico di Torino, Torino, Italy

The Euler equations that describe the steady supersonic flow can be reformulated in order to emphasize the role of propagating signals. From such formulations upwind criteria are derived for the approximation of derivatives by finite differences. Formulations based on the quasilinear form and the divergence form of the governing equations are considered. A numerical procedure based on these formulations is used as a tool for understanding the inviscid physics of the flow about a pointed cone at incidence. The generation and development of embedded crossflow shocks and related spiral entropy singularities are investigated.

Introduction

THE flow of a compressible inviscid fluid is described by the Euler equations. For unsteady or fully developed steady supersonic flows, these equations are hyperbolic with respect to time or an appropriate space coordinate (along which the fluid speed is supersonic), respectively. The theory of characteristics reveals the role played by propagation of signals. Namely, the evolution of the flow along the hyperbolic coordinate z is determined by signals carried over characteristic rays issued from suitable points on an initial data plane z_0 and merging at the point to be computed at $z = z_0 + Dz$.

The Euler partial differential equations can be written in divergence form (which is the obvious way of stating conservation principles) or rearranged to put the wave-like nature of the flows into evidence (that is, emphasizing the convection of signals originated "upwind"). Different upwind formulations can be conceived before any discretization. In any case, however, they lead to upwind codes, which best describe convection of signals.

Current in the literature are formulations stemming from the quasilinear form and from the divergence form of Euler's equations. Most of the efforts have been addressed to unsteady flows.

Less attention has been paid to steady supersonic flows. In particular, complete formulations and related numerical procedures founded on the quasilinear equations have been proposed in Refs. 1, 2, and 3. As regards the divergence form of the governing equations, some suggestions have been provided in Ref. 4, and a fully developed procedure for the two-dimensional steady supersonic flow can be found in Ref. 5. This methodology is based on the "flux-difference splitting" idea that, in turn, has been largely applied in the domain of unsteady flows.

In the present paper, we briefly outline the two-dimensional flux-difference splitting procedure proposed in Ref. 5 and then show how to extend these concepts to the three-dimensional problem. We also propose a hybrid formulation conceived as a blend of the "lambda" formulation (based on the quasilinear form of the governing equations and presented in Ref. 2) and of the conservative flux-difference splitting formulation. Finally, we apply the related numerical methodologies to the flow about a pointed circular cone at high incidence. Generation and development of embedded crossflow shocks and entropy singularities appear to be well described.

Received May 22, 1987; revision received Feb. 4, 1988.

*Research Scientist, Department of Aeronautical and Space Engineering.

†Professor, Department of Aeronautical and Space Engineering. Associate Fellow AIAA.

Flux-Difference Splitting

Here, we recall the basic ideas about the flux-difference splitting (FDS) for the simple case of the two-dimensional steady supersonic flow. For the sake of brevity and simplicity, we consider the governing equations written in a physical Cartesian frame (x,z). Later on, when dealing with the three-dimensional problem, a suitable transformation of coordinates will be used.

The governing equations written in the divergence form are

$$f_x + h_z = 0 \tag{1}$$

where f and h represent fluxes

$$f = \begin{vmatrix} \rho u \\ p + \rho u^2 \\ \rho uw \end{vmatrix}, \qquad h = \begin{vmatrix} \rho w \\ \rho uw \\ p + \rho w^2 \end{vmatrix}$$

The first of Eqs. (1) is of the continuity equation; the second and the third are projections of the vector momentum equation along the directions of the Cartesian coordinates (x,z). The energy equation is replaced here by the overall constancy of total enthalpy. Let the z-velocity component w be supersonic. Thus, the coordinate z is the hyperbolic one; the marching technique is carried out along it, and the initial data are prescribed over the other coordinate x.

Following the suggestion given in Ref. 6, we interpret the initial data (provided at a finite number of computational points) with piecewise uniform distributions of any flow property over the cell that extends half an interval ahead and behind a given computational point. With reference to Fig. 1, the distribution of the general flow property φ presents a discontinuity at $x_{N+1/2}$ in the middle of the interval (x_{N+1}, x_N). By proceeding along z, the jump collapses and generates the pattern of waves (1, 2, 3) that separates the new uniform regions (c,d) from the initial ones (a and b, containing the values at N and $N+1$, respectively). The breakdown of the discontinuity can be described exactly or approximately (see below). In any case, we may consider the difference of the flux f between the two points $N+1$ and N as split into three

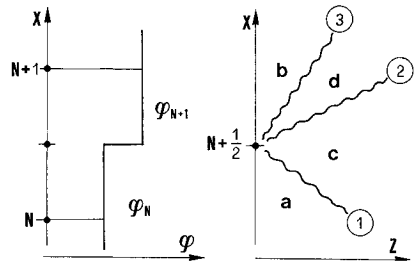

Fig. 1 Definition and solution of a Riemann problem.

terms:

$$D_N f = f_{N+1} - f_N = (f_b - f_d) + (f_d - f_c) + (f_c - f_a) \quad (2)$$

Each of the three terms on the right-hand side of Eq. (2) is related to the strength of the corresponding wave. Looking at the direction of propagation of the waves, we call $\overrightarrow{D_N f}$ the contribution of those terms related to the wave propagating with a positive velocity, and $\overleftarrow{D_N f}$ the terms corresponding to the other wave. Therefore, we have

$$D_N f = \overleftarrow{D_N f} + \overrightarrow{D_N f} \quad (3)$$

For instance, for the pattern shown in Fig. 1, it follows that

$$\overleftarrow{D_N f} = (f_c - f_a), \qquad \overrightarrow{D_N f} = (f_b - f_d) + (f_d - f_c)$$

Equations (2) and (3) describe the splitting of the difference of the flux. Such a splitting has to be performed at all intervals in order to proceed from the abscissa z_K, where the initial data are prescribed, to the next location $z_{K+1} = z_K + Dz$.

The ingredients $\overleftarrow{D_N f}$ and $\overrightarrow{D_N f}$ that appear in Eq. (3) can be used to build-up a numerical scheme of a desired order of accuracy. Limiting the accuracy to the first-order upwind scheme, the updating of the solution at the point N is given by

$$h_N^{K+1} h_N^K + (h_z)_N^K Dz = h_N^K - (f_x)_N^K Dz$$
$$= h_N^K - (\overrightarrow{D_{N-1} f} + \overleftarrow{D_N f}) Dz/Dx \quad (4)$$

Here, the derivative $(f_x)_N^K$ has been approximated with those contributions of the difference of the flux f in the two neighboring intervals that are flowing toward the point N. Once the flux h_N^{K+1} is known, any flow property can be obtained by a proper decoding from this value and from the constant total enthalpy condition.

Solution of the Riemann Problem

The collapse of the discontinuity shown in Fig. 1 is described by the equations of motion [Eqs. (1)]. The prediction of this phenomenon can be carried out exactly, according to well-known procedures reported in textbooks. Because of the nonlinearity of the equations, the "acoustic" waves (1 and 3) can be shock waves. In this case, the computation of the exact solution (by iteration) is tedious and time consuming. As mentioned in Ref. 7, however, we may simplify the problem by considering the transition through the acoustic waves as isentropic. This is the basic hypothesis proposed in Ref. 8 for the unsteady flow, but there the physical interpretation of the solver is different.

It is convenient to write the quasilinear equations under the assumption of isentropic flow and by selecting as dependent variables the logarithm of the pressure [$P = \ell n(p)$] and the slope of the streamlines ($\sigma = u/w$). A classical rearrangement of these equations provides the characteristic slopes:

$$\lambda_1 = (w^2\sigma - a^2\beta)/(w^2 - a^2), \qquad \lambda_3 = (w^2\sigma + a^2\beta)/(w^2 - a^2)$$

where a is the speed of sound and $\beta = \sqrt{M^2 - 1}$. The compatibility equations are

$$R_{1z} + \lambda_1 R_{1x} = 0, \qquad R_{3z} + \lambda_3 R_{3x} = 0 \quad (5)$$

The signals (R_1, R_3) are the Riemann invariants for the steady supersonic flow. Their definition in a differential form is given by

$$dR_1 = dP - \frac{\gamma w^2}{\beta a^2} d\sigma, \qquad dR_3 = dP + \frac{\gamma w^2}{\beta a^2} d\sigma \quad (6)$$

Through a classical integration we have the usual definition:

$$R_{1/3} = \sqrt{\frac{\gamma+1}{\gamma-1}} \tan^{-1}\left(\sqrt{\frac{\gamma-1}{\gamma+1}}\beta\right) - \tan^{-1}(\beta) \mp \tan^{-1}(\sigma) \quad (7)$$

We may now proceed to the solution of the Riemann problem. The matching conditions across the acoustic waves (1 and 3) require conservation of entropy (according to our assumption) and of the Riemann invariant [Eqs. (6) and (7)] convected along the characteristic that crosses the wave [Eq. (5)]. Across the contact surface (wave 2), pressure and streamline slope remain equal. Therefore, with reference to Fig. 1, we may write the following conditions:

$$R_{3c} = R_{3a}, \qquad S_c = S_a$$
$$P_c = P_d, \qquad \sigma_c = \sigma_d$$
$$R_{1d} = R_{1b}, \qquad S_d = S_b \quad (8)$$

The above six relationships lead to the prediction of the six unknowns [P, σ, S in regions (c,d)] on the basis of the prescribed value in the regions (a,b). The solution of Eqs. (8) is not simple at all from an algebraic point of view, owing to the complicated definition of the Riemann invariants [Eq. (7)]. The penalty to be paid in computer time may be unacceptable. In order to overcome this problem, we may consider a linearized version of Eq. (7), obtained directly from Eqs. (6). By doing this, the previous set of Eqs. (8) becomes

$$P_c + K_a\sigma_c = P_a + K_a\sigma_a, \qquad S_c = S_a$$
$$P_c = P_d, \qquad \sigma_c = \sigma_d$$
$$P_d - K_b\sigma_d = P_b - K_b\sigma_b, \qquad S_d = S_b \quad (9)$$

where

$$K = \frac{\gamma w^2}{\beta a^2}$$

The algebraic solution of Eqs. 9 is simple and fast.

More details, especially in the case of a zero-slope characteristic (sonic transition) embedded into an acoustic wave, are reported in Ref. 5.

Once the Riemann problem is solved in each interval, and the splitting is operated, we can proceed to the evaluation of the fluxes in the regions (c,d) and to the integration scheme [Eq. (4)].

FDS Formulation in Three-Dimensional Flows

Here, we outline the extension of the FDS formulation to the three-dimensional problem, with specific reference to the steady supersonic flow about a slender body.

We have closely followed the suggestions given in Ref. 9 as regards the geometrical problems and related definitions of the frames of reference. In particular, the Cartesian frame of reference (x,y,z) is introduced first. Then, the curvilinear

coordinates (ρ,θ,ζ) are defined as

$$\rho = \rho(x,y,z), \qquad \theta = \theta(x,y,z), \qquad \zeta = z \tag{10}$$

This second frame is introduced for mapping purposes, and the coordinates (ρ,θ) lie on a constant z-plane. Specifically, the contour of the cross section of the body should be represented by a constant ρ-line or depart slightly from it. Because in general the transformation provided by Eqs. (10) is based on a conformal mapping,[9] the curvilinear coordinates (ρ,θ) will be orthogonal to each other. A third and final frame describes the computational domain. The radial coordinate is normalized on the basis of the values at the body $[\rho = b(\theta,\zeta)]$ and at the bow shock $[\rho = c(\theta,\zeta)]$. The latter will be treated explicitly as a discontinuity, so that its location will be completely defined. Such a frame is defined as

$$X = \frac{\rho - b}{c - b}, \qquad Y = \theta, \qquad Z = \zeta$$

In general, the (X,Y) coordinates are not orthogonal in the (x,y) plane.

The Euler equations for the steady-state supersonic flow are written in the divergence form on the final computational frame (X,Y,Z), retaining the original Cartesian velocity components, so that the strong conservation form can be preserved.

Then, we define two sets of Riemann problems, one over DX intervals and another over DY intervals. They are easily solved by following the procedure outlined for the two-dimensional case. Additional features are introduced to account for the third space coordinate and the nonorthogonality of the grid.

Once the Riemann problems are solved, the differences of the fluxes defined on the cross-section plane (constant Z) over the grid intervals DX and DY are split. At this point, we can proceed with an integration scheme to update the solution along Z.

For brevity's sake, we limit ourselves to these short comments. The reader can find an exhaustive and detailed analysis of the procedure in a more extended version of this paper.[10]

Hybrid Formulation

Following the same line of action proposed for unsteady flows in Ref. 11, we begin with a few comments on the lambda and FDS formulations for steady supersonic flows.

The lambda formulation is appealing. The quality of the numerical results obtained using an explicit second-order scheme looks very good. The large number of numerical experiments reported in Ref. 9 and many others available in the literature support our personal experience on this matter. Good accuracy also means that the computational grid can be kept rough with savings in computing memory and time. Furthermore, the formulation based on the quasilinear equations simplifies the coding. Unfortunately, the numerics based on a plain lambda formulation does not capture shocks correctly. For three-dimensional supersonic flows about slender bodies, the bow shock can be fitted quite easily. The fitting of other shocks, embedded in the layer between the body and the bow shock, however, may result in severe coding problems.

The FDS formulation looks much less appealing than the lambda from any point of view, except the excellent capability in capturing shocks numerically with a neat and sharp transition, even with the plain first-order upwind scheme. A comparison of the FDS formulation with the lambda (of course, both of them coded consistently, for example, using a first-order scheme) shows that the FDS is less accurate. Therefore, more computational points are needed to reach a prescribed accuracy. In addition, the amount of algebraic operations is much higher. The result is a strong penalty in computing time. Moreover, the adoption of a second-order scheme in order to bring the accuracy to a satisfactory level leads to spurious numerical oscillations in the neighborhood of shock waves. This additional problem can be solved by introducing devices such as monotonicity criteria or flux limiters, which, in fact, degrade the accuracy to first order over the captured shock layer. In addition to the possible appearance of ambiguities near sonic transitions, the related numerical work is increased with a further penalty in computing time.

Consequently, it seems convenient to propose a hybrid formulation, sharing the positive features of the two discussed above, as follows. At each integration step, we explore the flowfield in order to recognize the presence of shock waves. Once they have been found, we consider two points ahead and two points behind any interval on which the shock transition has been detected. We label these points with an index IFORM = 1, whereas at all the other points in the computational domain we set IFORM = 0. Now we can proceed to the integration along the hyperbolic coordinate. At those points flagged by IFORM = 0, we use a second-order scheme based on the lambda formulation, whereas at the others (IFORM = 1) we apply the FDS formulation. In the latter case, we adopt the first-order scheme to assure monotonicity. The shock itself tends to swallow all steep gradients in its neighborhood so that the first-order accuracy is sufficient.

Such a hybrid formulation already has been successfully tested in significant test cases for all the unsteady flows,[12,13] and the numerical results we will present later on indicate the same positive evaluation for the steady supersonic case. Shock detection, however, still seems to be a difficult problem. In the present experiments, we have considered only shocks moving slowly through the computational domain and, therefore, the detection criterion is trivial; a shock occurs at any sonic transition going from supersonic to subsonic crossflow regimes. We are fully aware of the roughness of this detection and believe that more work has to be done on this point.

Numerical Experiment

As a first test to validate the above numerical technique, we have selected an interesting problem: the supersonic flow about a pointed circular cone at high incidence. The flow configuration is conical. We compute it asymptotically by starting from an initial configuration (the two-dimensional solution about a sharp cow lip[9]) and by integrating along the cone up to very large distances from the initial station, in the same spirit of the well-known time-dependent techniques. The numerical procedure uses the previously presented hybrid formulation and the explicit treatment of the bow shock.

The reader may find in the literature a very interesting and careful investigation on this problem.[14] Not only the bow shock, but also the embedded shock, which appears in the shock layer due to the high crossflow speed at high incidence, are explicitly fitted there. Therefore, we think that the description of phenomena such as the separation and circulation spiral shown in Ref. 14 and due to the vorticity generated by the crossflow shock can be assumed as a reliable benchmark for a new capturing procedure.

The following numerical exercise is not an end in itself. Through it we get a better understanding of the formation and development of vortices about bodies with smooth geometries, under the assumption of no viscosity.

Comments on the Numerical Results

We present here results relative to one of the cases reported and discussed in Ref. 14. The half-angle of the circular cone δ is equal to 10 deg, and the freestream Mach number M_∞ is equal to 2. We will show results for increasing values of the angle of attack α and focus our attention on the conical configurations represented on an (x,y) plane normal to the axis z of the cone. In particular, we will show isobar and streamline patterns. The latter are the projections on the (x,y)

plane of the paths of particles entering into the shock layer at the bow shock. Such a trace is obtained by integrating the already computed slopes of the streamlines on the (x,y) plane.

We start with no incidence ($\alpha = 0.0$ deg, Fig. 2). The configuration is trivial (radial streamlines and circular isobars). Each particle moves toward the body on a meridional plane and reaches the body asymptotically.

At a very small incidence ($\alpha = 1$ deg) the picture is not different except on a very thin layer near the body (Fig. 3). Even a small incidence generates a crossflow about the body. The pressure is not constant at the body anymore but decreases monotonically from the windward to the leeward side. Moreover, the streamlines show a sudden tangential deflection near the body. Their pattern around the leeward side is enlarged in Fig. 4 where we can note the formation of the entropy singularity, a sink where all the particles captured by the bow shock tend to concentrate and where, of course, the entropy level is not defined univocally.

By increasing the angle of attack, the axisymmetric pattern of pressure and of streamlines is completely lost all over the shock layer. The configuration at $\alpha = 10$ deg is shown in Fig. 5. The pressure at the body is no longer monotonic, as for smaller incidences, but a recompression occurs near the entropy singularity. The latter becomes more prominent (Fig. 6). The shape of the streamlines is quantitatively, but not qualitatively, changed.

A slight increase in incidence pushes the entropy singularity up from the body into the shock layer, as suggested many years ago.[15] Such a lifting clearly appears at $\alpha = 16$ deg (Fig. 7). Note that the leeward side looks like a dead-water region with a flat pressure distribution and negligible crossflow velocity. This last fact is responsible for the high number of integration steps (or large distance from the initial station) needed to generate the fully developed conical configurations. The enlargement of Fig. 8 clearly shows the lifted entropy singularity.

Until now, the crossflow has become more and more relevant with the incidence. At $\alpha = 16$ deg, it is still subsonic, but a peak of the crossflow Mach number is slightly below the sonic level. Thus, we may easily anticipate the formation of a crossflow supersonic bubble, ending in a shock if the incidence increases. This is just what we see at $\alpha = 19$ deg. Note that the shock extends radially for a very short distance; it is rather strong at the body and soon vanishes above it. The first consequence is the strong vorticity left in the stream behind the shock itself. We note the similarity with the two-dimensional transonic flow about a circular cylinder.[12,13] The high dissipation experimented by the flow particles crossing the shock at its root prevents them to reach a crossflow stagnation point on the symmetry plane. In fact, these particles separate from the body. The configuration is shown in Fig. 9

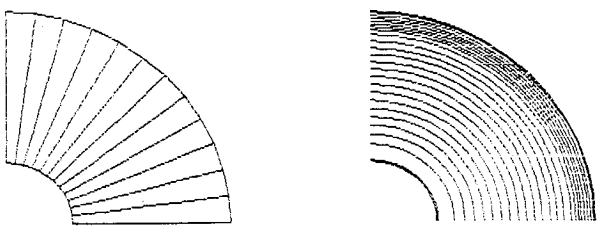

Fig. 2 Streamlines and isobars ($\delta = 10$ deg, $\alpha = 0$ deg).

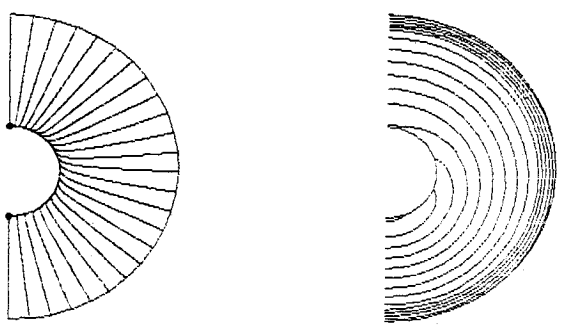

Fig. 3 Streamlines and isobars ($\delta = 10$ deg, $\alpha = 1$ deg).

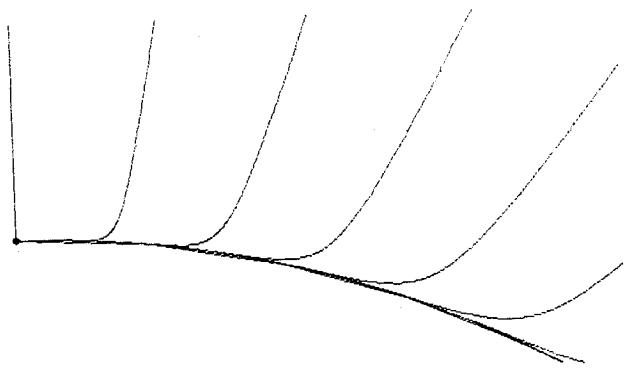

Fig. 4 Details of the streamlines near the entropy singularity ($\delta = 10$ deg, $\alpha = 1$ deg).

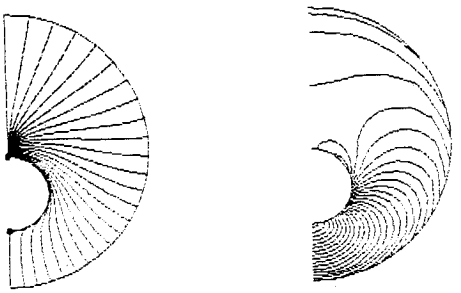

Fig. 5 Streamlines and isobars ($\delta = 10$ deg, $\alpha = 10$ deg).

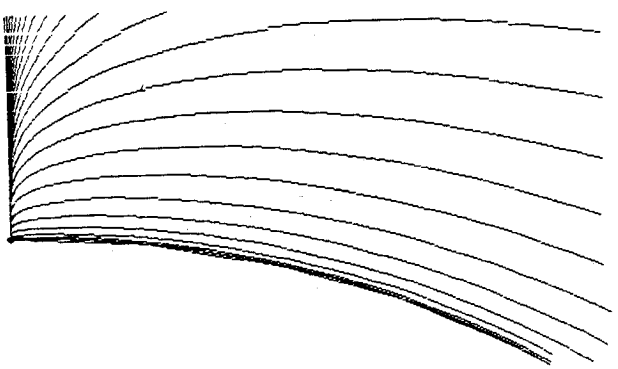

Fig. 6 Details of the streamlines near the entropy singularity ($\delta = 10$ deg, $\alpha = 10$ deg).

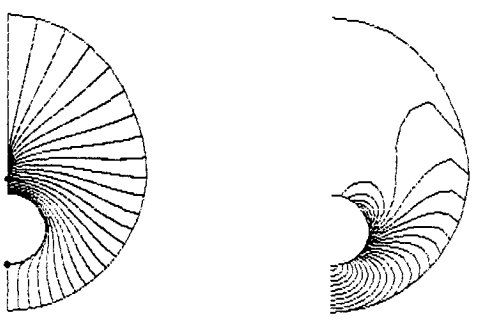

Fig. 7 Streamlines and isobars ($\delta = 10$ deg, $\alpha = 16$ deg).

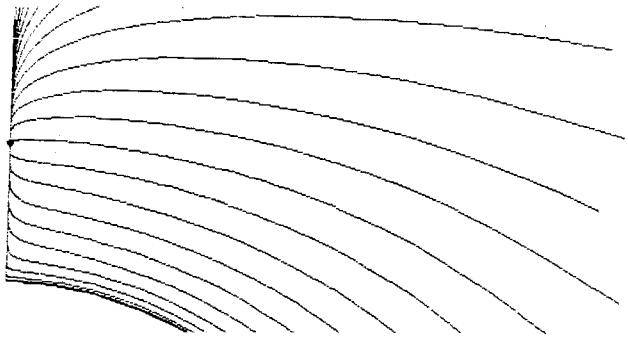

Fig. 8 Details of the streamlines near the entropy singularity ($\delta = 10$ deg, $\alpha = 16$ deg).

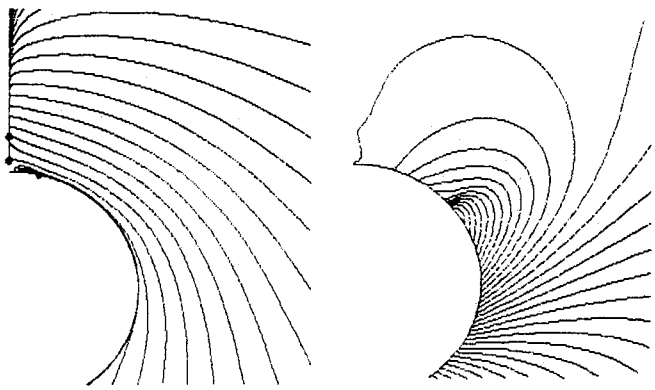

Fig. 9 Streamlines and isobars ($\delta = 10$ deg, $\alpha = 19$ deg).

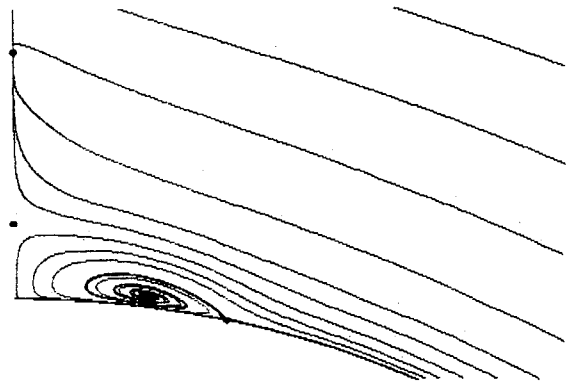

Fig. 10 Details of the streamlines near the entropy singularity and the spiral ($\delta = 10$ deg, $\alpha = 19$ deg).

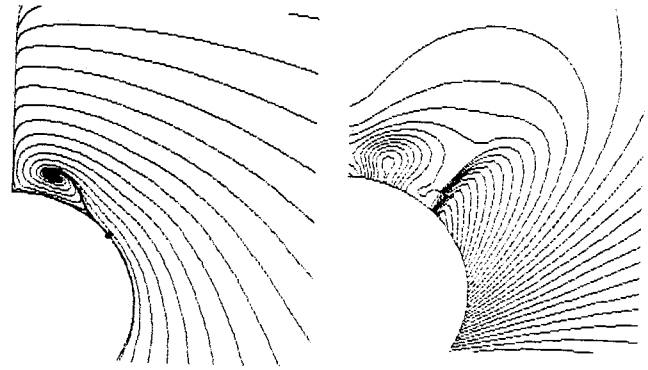

Fig. 11 Streamlines and isobars ($\delta = 10$ deg, $\alpha = 25$ deg).

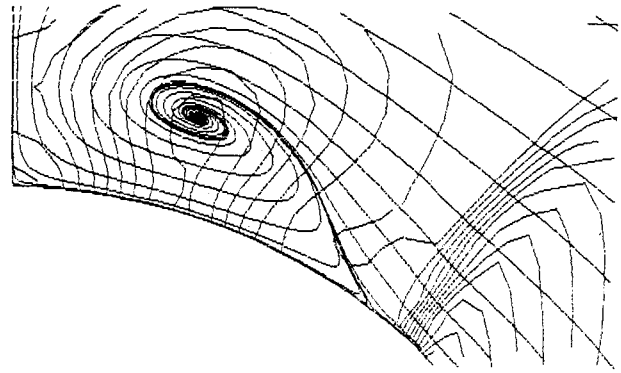

Fig. 12 Details of the streamlines and the isobars in the spiral ($\delta = 10$ deg, $\alpha = 25$ deg).

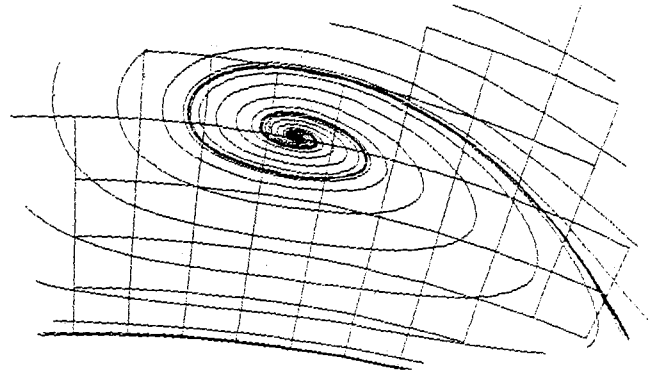

Fig. 13 Detailed view of the spiral and the grid ($\delta = 10$ deg, $\alpha = 25$ deg).

where the crossflow shock is barely detectable in the isobars picture. In the enlargement of Fig. 10, we can distinguish clearly two separate regions in the shock layer: the flow converging toward the lifted entropy singularity that covers most of the shock layer region, and the narrow region near the body with the highly rotational flow that separates behind the crossflow shock. Despite the graphic analogy between the present flow and the steady recirculating flow bubble in the two-dimensional flow about the cylinder, it is worth noting their physical differences, due to the different role played by the hyperbolic coordinate. Here, the separation generates a spiral, and the particles captured by it converge toward its center, generating a second entropy singularity (the spiral singularity). The latter reduces the rate of lifting of the first one. An additional crossflow stagnation point appears on the leeward symmetry plane that separates the two streams flowing into the two singularities. The outer stream carries the weak vorticity induced by the bow shock, whereas the inner one is dominated by the strong vorticity generated at the embedded crossflow shock. From the numerical point of view, we observe that the FDS procedure is now applied at the crossflow shock and generates the entropy gradients responsible for the formation of the spiral.

As the incidence is further increased, the vorticity generated at the crossflow shock becomes predominant inside the shock layer. Now, the rotationality of the spiral singularity is so large that its rolling effect can reach the first lifted singularity and sweep it away toward the center of the spiral. The flow configuration for a very high angle of attack ($\alpha = 25$ deg) is shown in Fig. 11. The crossflow shock is now rather evident. The spiral entropy singularity has completely swallowed the other singularity, and all of the flow particles converge now

into its center. Observe the streamline that detaches from the body behind the crossflow shock (Fig. 12). Its root is reached by two types of particles: the ones coming from the windward side of the bow shock that go through the crossflow shock, and the ones coming from the leeward side of the bow "shock," which is actually an expansion wave. The former have experimented the highest increase in entropy; the latter have the same entropy as in the freestream. Therefore, the double streamline separating from the body is a contact surface. Note also in Fig. 12 the typical Ω shape of the isobars. The center of the vortex coincides perfectly with the core of the isobars; we can consider this as a testimony of the correctness of the calculation. A detailed view of the spiral and the computational grid are shown in Fig. 13. Note that by zooming into the spiral as much as we like, its shape remains unchanged.

We conclude with an experiment suggested by the two-dimensional transonic flow about a circular cylinder where, as shown in Ref. 13, vortices are shed alternatively from the upper and lower side. Here, we may expect a similar phenomenon to occur along the hyperbolic coordinate z. Starting from the results obtained over the half-plane for $\alpha = 25$ deg, we have reproduced them symmetrically on the opposite half-plane. Then, we have carried out the integration all over the plane for a large number of steps. We did not notice any departure from the conical picture at all. Furthermore, we changed the direction of the upstream flow by adding a yaw and decreasing the angle of attack, so that the effective incidence remained constant. After a strong rearrangement of the flowfield, a new stable conical configuration appeared that is exactly the previous one, properly rotated. In conclusion, the configuration is stable.

Most of the considerations and comments about these physical phenomena descend from the original investigations shown in Ref. 14. Here, we would like to point out the remarkable agreement (not only qualitative but also quantitative) of our results with those reported in Ref. 14. Since we take Ref. 14 as a benchmark, we see the above calculation as a good step toward validating our proposed technique.

Before closing, we recall that the grid size (radial-peripheral intervals) used in our computations over the half-plane has been either 18×36 or 36×72, with a rather strong stretching in the radial direction near the body to impose local resolution.

Conclusions

Two upwind formulations are used for the numerical analysis of steady supersonic flows. One (based on the quasilinear form of the governing equations) is well known as the lambda formulation. The other is based on the flux-difference splitting idea, which allows shock waves to be captured correctly. It is also the only "conservative" upwind formulation proposed so far that works for the steady supersonic flow.

In this paper, we introduced a blend of the previous two, to take advantage of their positive features. The technique has been efficient and robust in the present application. Further work will be devoted to test it for more complicated shock patterns (for instance, a three-dimensional supersonic corner flow) and to generalize the shock detection.

References

[1]Walkden, F., Caine, P., and Laws, G. T., "A Locally Two-Dimensional Numerical Method for Calculating Three-Dimensional Supersonic Flows," *Journal of Computational Physics*, Vol. 27, April 1978, pp. 103–122.

[2]Moretti, G., "The Lambda Scheme," *Computers and Fluids*, Vol. 7, No. 3, Sept. 1979, pp. 191–205.

[3]Chakravarthy, S. R., Anderson, D. A., and Salas, M. D., "The Split-Coefficient Matrix Method for Hyperbolic Systems of Gas Dynamic Equations," AIAA Paper 80-0268, Jan. 1980.

[4]Roe, P. L., "Approximate Riemann Solvers, Parameters, Vectors and Difference Schemes," *Journal of Computational Physics*, Vol. 43, No. 2, Oct. 1981, pp. 357–372.

[5]Pandolfi, M., "Computation of Steady Supersonic Flows by a Flux-Difference Splitting Method," *Computers and Fluids*, Vol. 10, Jan. 1985, pp. 37–46.

[6]Godunov, S. K., "A Finite Difference Method for the Numerical Computation of Discontinuous Solutions of the Equations of Fluid Dynamics," *Matematicheskii Sbornik*, Vol. 47, No. 3, 1959, pp. 271–290.

[7]Pandolfi, M., "A Contribution to the Numerical Prediction of Unsteady Flows," *AIAA Journal*, Vol. 22, May 1984, pp. 602–610.

[8]Osher, S. and Solomon, F., "Upwind Difference Schemes for Hyperbolic Systems of Conservation Laws," *Mathematics of Computation*, Vol. 38, April 1982, pp. 339–377.

[9]Moretti, G., "Calculation of Three Dimensional Inviscid Supersonic Steady Flows," NASA CR-3573, June 1982.

[10]Botta, N. and Pandolfi, M., "Upwind Formulations for the Euler Equations in Steady Supersonic Flows," AIAA Paper CP 874, June 1987, pp. 527–536.

[11]Pandolfi, M., "The Merging of Two Different Ideas: A Shock Fitting Performed by a Shock Capturing," *Proceedings of the Computational Fluid Dynamics Symposium*, Tokyo, Sept. 1985.

[12]Pandolfi, M., Larocca, F., and Tamiru Ayele, T., "A Contribution to the Numerical Prediction of Transonic Flows," GAMM Workshop on the Numerical Solution of the Euler Equations, Rocquencourt, June 1987.

[13]Pandolfi, M. and Larocca, F., "Transonic Flows About Circular Cylinders," *Computers and Fluids* (to be published).

[14]Marconi, F., "The Spiral Singularity in the Supersonic Inviscid Flow Over a Cone," *AIAA Journal*, Vol. 22, Aug. 1984, pp. 1048–1055.

[15]Ferri, A., "Supersonic Flow Around Circular Cones at Angles of Attack," NACA Rept. 1045, 1951.